J. Shanghai Jiao Tong Univ. (Sci.), 2019, 24(2): 176-183
https://doi.org/10.1007/s12204-019-2053-y

Characteristics of the Internal Waves Generated by a Towed Model with Rotating Propeller Under a Strong Halocline

DUAN Ningyuan[1] (段宁远), *CHEN Ke*[1*] (陈　科), *WANG Hongwei*[2] (王宏伟), *YOU Yunxiang*[1] (尤云祥)
(1. State Key Laboratory of Ocean Engineering, Shanghai Jiao Tong University, Shanghai 200240, China;
2. China Ship Development and Design Center (Shanghai), Shanghai 201108, China)

Abstract: Experiments are performed on the internal waves (IWs) generated by a towed model with rotating propeller in a density-stratified fluid with linear halocline; the Reynolds number ranges from 7 000 to 84 000, and the Froude number ranges from 0.7 to 8.1. The wave speed, amplitude and patterns are investigated on the basis of the multi-channel conductivity probe array technology and the cross correlation analysis method. It is shown that the propeller advances the transition from the body-generated IWs to the wake-generated IWs. Before the transition, the IWs are stationary to the translational model. An extra V-shaped wave with a narrow opening angle is generated by the propeller and the wave amplitude becomes larger with the increase of the thrust momentum, indicating that the propeller produces body and wake effects at the same time before the transition. After the transition, the Froude number associated with the wave speed drops down and fluctuates within 0.4—1.5, showing that the IWs are nonstationary to the model. The interaction of the drag momentum and the thrust momentum changes the characteristics of the wave amplitudes and patterns. The wave amplitude no longer simply grows with the Froude number but depends on the contrast of the drag momentum and the thrust momentum. Experimental results show that the most obvious contrast of the wave pattern contour maps appears when the drag momentum and the thrust momentum have the largest difference if other conditions are the same. When the ratio of the drag momentum to the thrust momentum is within 1—10, the wake can be considered as zero-momentum, meaning that the momentum difference is not enough to generate large scale structures in the wake.
Key words: internal wave (IW), stratified fluid, momentum wake, self-propelled model
CLC number: O 352　　**Document code:** A

0 Introduction

Internal wave (IW) is a common phenomenon in a stratified ocean. When a submerged object moves in the stratified fluid, its body and wake drive water clusters away from the equilibrium position, triggering the oscillations of water clusters and generating the IWs behind its track. Keller and Munk[1] introduced the kinematic line approach to predict the IW patterns generated by a moving point source in a thermocline. For a certain mode, the transverse wave and the divergent wave exist simultaneously when the translational speed is less than the critical phase velocity, while only the divergent wave exists in the horizontal wave pattern conversely. This kinematic line theory cannot obtain quantitative data such as IW amplitudes for the dynamics of IWs. Besides, a horizontally translational point source does not fully agree with the practical phenomena, because it is usually an object with a certain volume.

Robey[2] conducted the experiments of IWs generated by a sphere towed horizontally in a density-stratified fluid. A classification of excitation sources proposed by Robey includes two types: body-generated and wake-generated IWs. The body-generated IWs, which are stationary to the moving sphere, are generated by the sphere itself and the following separation bubble. The wake-generated IWs, which are nonstationary to the sphere, are produced by a variety of complex excitation sources. Generally, the IWs generated by the towed sphere contain the body-generated and wake-generated IWs, but there is a transition from the body-generated IWs to the wake-generated IWs with the growth of the translational speed. The critical speed is characterized by the Froude number. Studies on a towed sphere show that the transition of dominant IWs occurs when the Froude number is 2[2-7]. The wave amplitude before the transition has a peak value when the Froude number is within 0.7—0.8, and the wave amplitude grows linearly with the Froude number after the transition. Wang et al.[8] further investigated four towed

Received date: 2017-11-06
Foundation item: the National Natural Science Foundation of China (No. 11802176)
∗**E-mail:** raulphan@sjtu.edu.cn

models with different aspect ratios and observed that the critical Froude number has a linear growth relation against the aspect ratio. For the wave amplitudes after the transition, the slopes of different models are very close to each other, indicating that the wake-generated IWs are little influenced by the body length. Though studies on towed models are comprehensive, the actual underwater vehicle is driven by a propeller installed at the stern. Several studies have focused on the wakes influenced by a propeller, showing that the existence of propeller changes the velocity field which influences the formation of IW excitation source[9-13]. Wang et al.[14] conducted the experiments of IWs generated by a self-propelled model in a stratified fluid. The IWs generated by self-propelled model have different features as compared with those of towed models. The transition from body-generated IWs to wake-generated IWs takes place earlier than that of towed model, and the wave amplitude after the transition fluctuates within a range rather than increases with the moving speed.

Unlike the body-generated IWs, the wake-generated IWs are excited by the wake produced by the interaction of the body and its surroundings. From the view of momentum, the towed model provides a drag momentum to the environmental fluids while the self-propelled model has no momentum flux due to the thrust momentum generated by its propeller in the opposite direction to the drag momentum. The zero-momentum wake formed by the self-propelled model contains very low energy and cannot produce large-scale structures to generate large wave amplitudes, which is verified in the experiments of Wang et al[14]. However, when the vehicle moves unsteadily in a stratified fluid, the drag momentum and the thrust momentum are not balanced to form a non-zero momentum wake. It is possible for the development of an IW with large amplitude under such a condition. Thus, the experimental investigation is conducted in this paper on the IWs generated by a towed model under different propeller effects in a strongly stratified fluid so as to show the characteristics of the transition, wave amplitude and wave patterns of the IWs excited under the unsteady state of the self-propelled vehicle. The purpose of the research is to promote the understanding of hydrodynamic wakes behind the underwater vehicle for applications in the antisubmarine detection.

1 Experimental Setup

The experiments are conducted in a rectangular water tank (length: 12 m; width: 1.2 m; depth: 1 m). The tank has two mushroom-shaped inlets at the bottom. The coordinate system is defined with $x_0 = 0$ at the left end of the tank, $y_0 = 0$ at the center of the width and $z_0 = 0$ on the water surface. The total water depth (H) is 0.8 m. The model used in this paper is the standard SUBOFF model with a diameter (D) of 7 cm and an aspect ratio of 8. The five-blade propeller with a diameter of 3 cm is fixed at the stern, and it is controlled by an external direct-current (DC) power supply. The model is positioned in the center of the width. Its central axis is at $z = h = 0.4$ m and its head is located at $x = x_1 = 1.5$ m. The guiding line above the model is used for navigating along a straight line, while the towing line under the model driven by a cyclic motor is used to tow the model at a constant speed. Two arrays of micro-scale electronic conductivity probes with a sampling frequency of 20 Hz are used as the dynamic measure equipment. They are sensitive enough because their period (0.05 s) is shorter than the typical internal wave period (about 3 s). These sensors are calibrated by different salt solutions before the experiments and the linear relationships between solution densities and electrical signals are used to process the original data. The first array including 23 probes is located at $x = x_2 = 4$ m and arranged symmetrically along y axis with an interval of 5 cm. These 23 probes are marked as $\{E_0, E_{\pm1}, \cdots, E_{\pm11}\}$, and E_0 is located at the mid-point of the cross section. The distance between the second array and the first array in x axis is $\Delta x = 150$ cm. Eight probes that compose the second array are arranged symmetrically along y axis at ±10, ±20, ±30 and ±40 cm, identified as $F_{\pm2}$, $F_{\pm4}$, $F_{\pm6}$ and $F_{\pm8}$, respectively. Two arrays are both located at $z = z_p = 25$ cm in depth where the maximum Brunt-Vaisala (B-V) frequency is located in the experiments. The first array is used for measuring the IW patterns on the horizontal plane, while the second array is used for the correlation speed in different vertical sections. The experimental system is shown in Fig. 1(a).

As shown in Fig. 1(b), the model has two kinds of

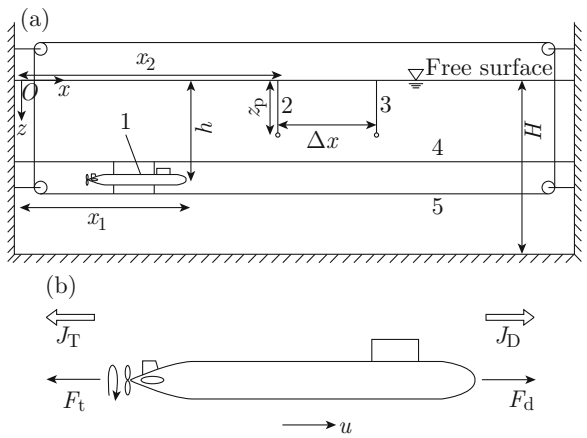

1—SUBOFF model, 2—The first array of probes, 3—The second array of probes, 4—Guiding line, 5—Towing line

Fig. 1 Sketch of the experimental system (side view) and the body-fluid interaction

momentum effects on the surrounding fluid. In the movement with a translational speed (u), the resistance of the model hull produces a forward force (F_d) while the thrust of the propeller excites a backward force (F_t); therefore, the drag momentum (J_D) and the thrust momentum (J_T) are generated by these two forces, respectively. In the past studies, only the drag momentum of the hull is considered. In this paper, three different J_T values are added to the towed model to investigate their effects on the characteristics of IWs.

Two-bucket method is used to acquire the stratified fluid. Firstly, 0.25-m-deep fresh water with a density of 0.998 g/cm^3 bumps into the tank. After that, 0.55-m-deep saline water with a density of 1.022 g/cm^3 is injected into the tank through two mushroom-shaped inlets at the bottom of the tank. The whole process is slow and steady and it needs 24 h. Finally, a 0.8-m-high three-layer fluid is obtained, with 0.2-m-high freshwater in the up layer, 0.5-m-high salt saline water in the bottom layer and a linear stratification about 10 cm around the interface. The purpose of this configuration is to compare the results with those of the literature[8,14]. The density (ρ) profile and its buoyancy frequency (N) are plotted in Fig. 2. The B-V frequency is calculated by $N = [-(g/\rho_0)(\mathrm{d}\rho/\mathrm{d}z)]^{1/2}$, where g is the gravitational acceleration and ρ_0 is the density of fresh water. It can be seen from the figure that the maximum frequency (N_max) takes place at a depth of 25 cm and its value is 2.13 rad/s.

As the self-propelled model moves steadily with a constant speed, the body drag and the propeller thrust are in balance and there is no net momentum imparted to the environment, leading to a zero-momentum condition. When the model is in unsteady motion, e.g., acceleration or deceleration, these two forces are not balanced and there exists a net momentum which may excite the large vortex structures that are the possible reason for generation of IWs. The formula calculating the momentum of body drag is[15-18]

$$J_\mathrm{D} = \frac{1}{2} C_\mathrm{D} u^2 S_\mathrm{D}, \tag{1}$$

where C_D is the drag coefficient (here $C_\mathrm{D} = 1$ for simplification), and $S_\mathrm{D} = \pi D^2/4$ is the cross-sectional area.

Owing to the difficulty of measuring the thrust momentum directly, an alternative method is applied in this paper. As mentioned earlier, the thrust momentum is equivalent to the drag momentum if the model is cruising steadily. Hence, the relation between the self-propelled speed and the voltage is determined to quantify the thrust momentum before the experiments. In the calibration, the model is only propelled by its propeller, and the speed is measured as the model moves steadily. Each voltage is repeated three times. Finally, the linear relation between the voltage and the self-propelled speed is obtained by data fitting, as shown in Fig. 3. The formula is

$$u_\mathrm{j} = 9.02U - 30.3, \tag{2}$$

where u_j is the self-propelled speed of model and U is the DC voltage.

Accordingly, the thrust momentum can be calculated by

$$J_\mathrm{T} = \frac{1}{2} C_\mathrm{D} u_\mathrm{j}^2 S_\mathrm{D}. \tag{3}$$

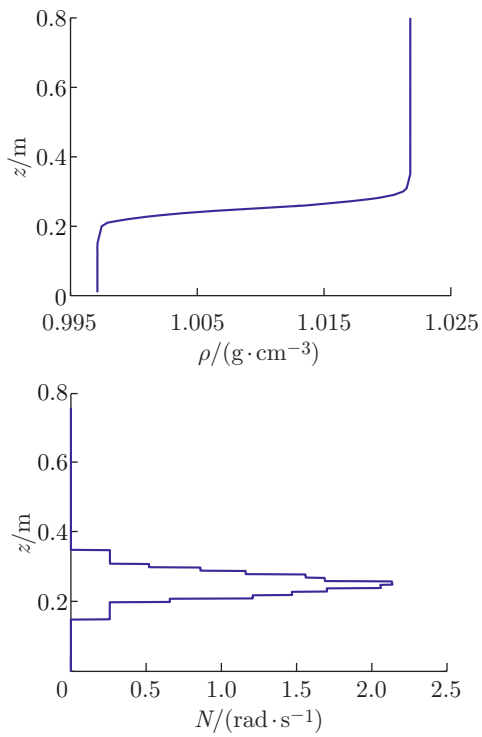

Fig. 2 Profiles of density and buoyancy frequency

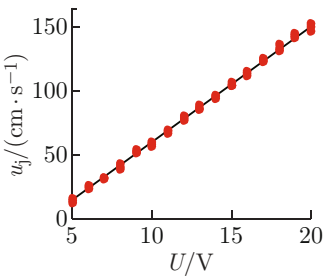

Fig. 3 Relation between the voltage and the self-propelled speed

For exploring the effect of the thrust momentum, three J_T values are considered to investigate the propeller effect on IWs. They are $J_\mathrm{T} = 1.9 \times 10^{-5}$, 1.7×10^{-4} and 1.1×10^{-3} m^4/s^2. In the experiments, the towing speed of the model ranges from 10 to 120 cm/s. Thus, the corresponding Froude number

($Fr = u/(DN_{\max})$) ranges from 0.7 to 8.1 and the Reynold number ($Re = uD/\nu$, where $\nu = 1\,\mathrm{mm}^2/\mathrm{s}$ is the kinematic viscosity) ranges from 7 000 to 84 000. The acquisition time of probe signals is 5 min for each run, and the waiting interval of two runs is no less than 30 min for that no disturbance has been detected and the density distribution has re-equilibrated.

2 Results and Discussion

2.1 Transition Characteristics

Here we discuss the transition characteristics that are closely related to the speed of IWs. The speed of IWs is obtained by the cross correlation analysis method. At first, the correlation between the probes sharing the same y position in two arrays is analyzed, and the propagation time (Δt) is adopted from the peak coefficient value. Then, the along-track speed in the experiments is calculated by $u_{\mathrm{iw}} = \Delta x/\Delta t$, where the distance between two arrays is $\Delta x = 150\,\mathrm{cm}$. According to the previous studies, the body-generated IWs are stationary to the translational body while the wake-generated IWs are nonstationary random waves whose speed is slower than the towing speed. Generally, the correlation speed u_{iw} is investigated through the dimensionless form, and it can be defined by the Froude number, $Fr_{\mathrm{iw}} = u_{\mathrm{iw}}/(DN_{\max})$. The result of Fr_{iw} versus Fr is shown in Fig. 4, where the along-track speeds at eight longitudinal sections are plotted.

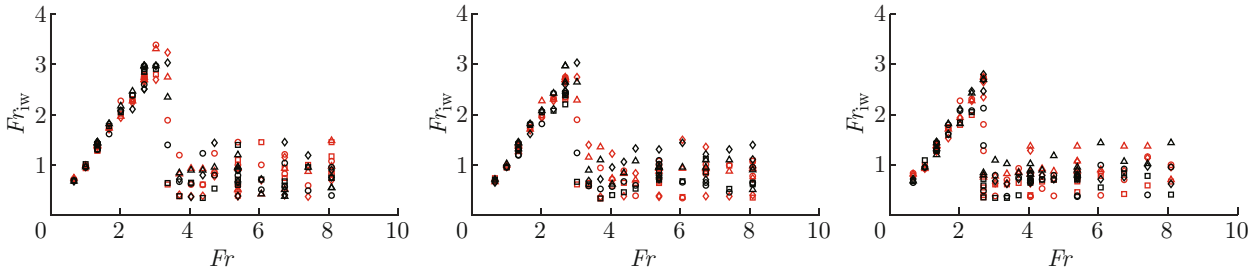

(a) $J_{\mathrm{T}} = 1.9\times10^{-5}\,\mathrm{m}^4/\mathrm{s}^2$ (b) $J_{\mathrm{T}} = 1.7\times10^{-4}\,\mathrm{m}^4/\mathrm{s}^2$ (c) $J_{\mathrm{T}} = 1.1\times10^{-3}\,\mathrm{m}^4/\mathrm{s}^2$

$\diamond E_{-8}$-F_{-8}, $\triangle E_{-6}$-F_{-6}, $\circ E_{-4}$-F_{-4}, $\square E_{-2}$-F_{-2}, $\square E_{+2}$-F_{+2}, $\circ E_{+4}$-F_{+4}, $\triangle E_{+6}$-F_{+6}, $\diamond E_{+8}$-F_{+8}

Fig. 4 The result of Fr_{iw} versus Fr

The transition characteristics can be seen from Fig. 4. Before the transition, Fr_{iw} for the IW correlation speed is equal to Fr for the towing speed, indicating that the IWs are stationary to the towed model. After the transition, Fr_{iw} at different sections drops down and fluctuates within 0.4—1.5 regardless of the towing speed, indicating that the IWs are nonstationary to the towed model. Such phenomenon is similar to the results of the towed sphere, slender body and self-propelled model.

Considering the model as a slender body with an aspect ratio of 8, the critical Froude number (Fr_{c}) is 3.4 when it is a towed model, and Fr_{c} is 2.95 when it is a self-propelled model[14]. However, the transition in this study occurs for the critical Froude number at 3.3, 3.0 or 2.7, as shown in Fig. 4. Obviously, the propeller effect causes the differences. For J_{T} at $1.9\times10^{-5}\,\mathrm{m}^4/\mathrm{s}^2$, Fr_{c} at 3.3 is closest to the towed model one as its propeller effect is the lowest among the three cases. For J_{T} at $1.7\times10^{-4}\,\mathrm{m}^4/\mathrm{s}^2$, Fr_{c} at 3.0 is close to the critical Froude number of the self-propelled model for J_{T} at $2.4\times10^{-4}\,\mathrm{m}^4/\mathrm{s}^2$. The smallest Fr_{c} at 2.7 is associated with the maximum J_{T} at $1.1\times10^{-3}\,\mathrm{m}^4/\mathrm{s}^2$. Table 1 gives a summary on Fr_{c} versus J_{T}

Table 1 shows that the higher the thrust momentum is, the earlier the transition occurs. In essence, the advance of transition from the body-generated IWs to the wake-generated IWs is a result of the growing strength of the wake that the propeller produces.

Table 1 Summary on Fr_{c} versus J_{T}

$J_{\mathrm{T}}\times10^4/(\mathrm{m}^4\cdot\mathrm{s}^{-2})$	Fr_{c}
0	3.4
0.19	3.3
1.7	3.0
2.4	2.95
11	2.7

2.2 Maximum Peak-Peak Wave Amplitude

The wave amplitude is another significant characteristic for the IWs. In this paper, the maximum peak-peak wave amplitude (A_{m}) is obtained from the first 120 s of the wave elevations in the first array. Its dimensionless form is defined as A_{m}/D. The relations for A_{m}/D versus Fr and A_{m}/D versus J_{nd} are plotted in Fig. 5, where $J_{\mathrm{nd}} = J_{\mathrm{D}}/J_{\mathrm{T}}$ stands for the contrast between the drag momentum and the thrust momentum while $J_{\mathrm{nd}} = 1.0$ represents that the drag momentum equals the thrust one.

The Froude number associated with the peak value of wave amplitude before the transition is denoted as Fr_{p}. As shown in Fig. 5(a), the wave amplitude has

a peak value for Fr_p at 1 before the transition ($Fr < Fr_c$), like the situation of the towed model and the self-propelled model. After the transition ($Fr > Fr_c$), the wave amplitude has a linear increase with the increase of Fr and the fitting line slope is 0.013 3, almost half of 0.026 which is proposed in Ref. [8]. This discrepancy is caused by different vertical distances between the model and the pycnocline.

In Fig. 5(c), before the transition, the wave amplitude also has a peak value for Fr_p at 1 and decreases with the increase of Fr. The discrepancy between Fig. 5(c) and Fig. 5(a) emerges after the transition. The wave amplitude does not have an expected growth with the increase of Fr immediately but it fluctuates within 0.05—0.06 until Fr at 6, which is different from the first case. Then, the wave amplitude begins to increase for Fr exceeding 6.

In Fig. 5(e), before the transition, the wave amplitude decreases with the increase of Fr and the maximum peak value occurs for Fr_p at 0.7. After the transition, the wave amplitude continues to decrease with the increase of Fr and does not have an explicit trend of growth.

Robey's explanation for the amplitude peak before the transition is that Fr_p indicates a resonance between the body moving speed and the environmental buoyancy frequency[2]. This resonant dynamic also occurs in the wave speed, showing that after the transition Fr_{iw} is close to Fr_p. In Wang's study and this work, Fr_{iw} fluctuates within 0.4—1.5 after the transition, which means that the resonance happens at not a single point but within a certain range. Here $Fr_p = 1$ and $Fr_p = 0.7$ are located in a resonance range of 0.4—1.5 and very close to 0.95 (the middle point). But it is remarkable that the wave amplitude associated with each Fr becomes larger with the increase of J_T before the transition, e.g., the A_m/D values are about 0.08, 0.1 and 0.19 when the J_T values are 1.9×10^{-5}, 1.7×10^{-4} and 1.1×10^{-3} m^4/s^2 respectively for Fr at 1.7.

The least square method is used to fit the A_m/D data before the transition. Three fitting lines can be obtained for each case. The expressions of the fitting lines are $A_m/D = 0.146Fr^{-1.03}$, $A_m/D = 0.164Fr^{-1.07}$ and $A_m/D = 0.308Fr^{-1.06}$, as shown in Fig. 5. All the values of A_m/D approximately decline in inverse proportion to the values of Fr, only different in the coefficients. This phenomenon indicates that the propeller effect before the transition amplifies the wave amplitude. Its effect acts as a coefficient in the relation of A_m/D versus Fr, and a high propeller effect leads to a bigger coefficient.

After the transition, in the previous studies, a self-propelled model moves in the fluid steadily, forming a non-momentum wake[12]. The non-momentum wake cannot induce large-scale structures, which is considered the main source of the wake-generated IWs. Thus the wave amplitude cannot have an explicit growth trend with the increase of Fr but it changes within 0.04—0.07[14].

In this paper, the situation is much more complicated. The wave amplitude in the first case shows a linear growth with Fr, like the situation of a towed model. The wave amplitude in the second case does not rise until Fr at 6, and in the third case it continues to decrease after the transition and does not have an obvious increase. Such difference also results from the propeller effect and is related to the momentum balance between J_D and J_T.

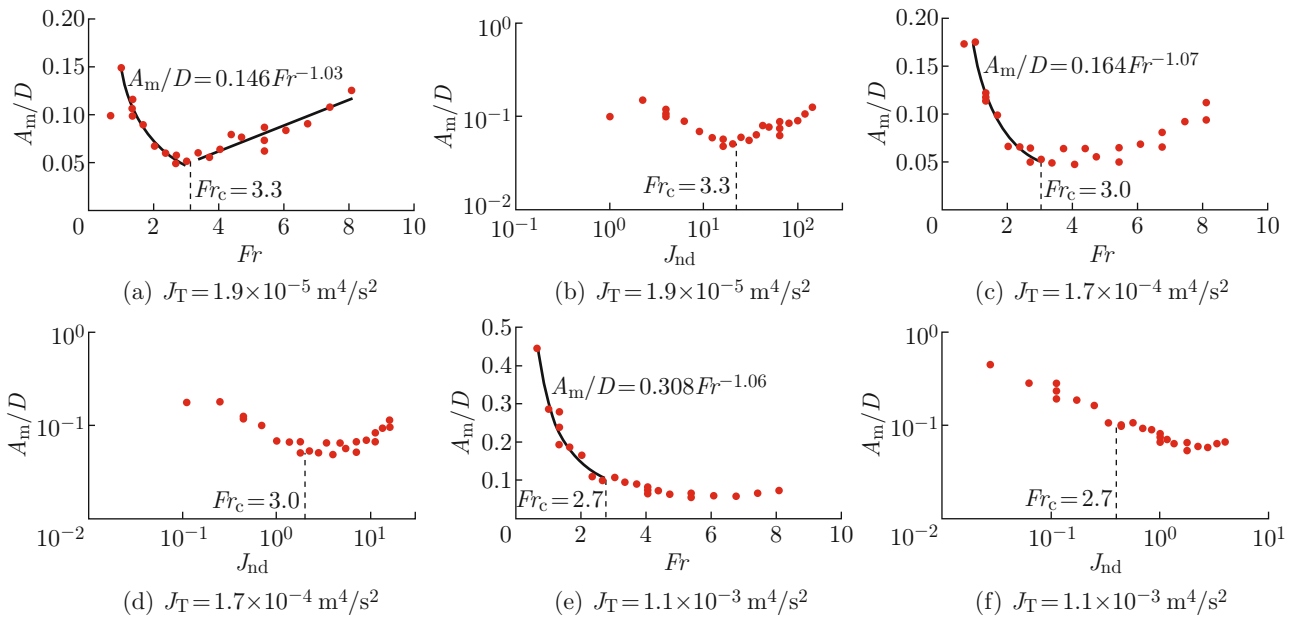

(a) $J_T = 1.9\times10^{-5}$ m^4/s^2 (b) $J_T = 1.9\times10^{-5}$ m^4/s^2 (c) $J_T = 1.7\times10^{-4}$ m^4/s^2

(d) $J_T = 1.7\times10^{-4}$ m^4/s^2 (e) $J_T = 1.1\times10^{-3}$ m^4/s^2 (f) $J_T = 1.1\times10^{-3}$ m^4/s^2

Fig. 5 The relations for A_m/D versus Fr and A_m/D versus J_{nd}

Previously, J_{nd} is introduced to show the momentum contrast. In the first case, the J_{nd} value corresponding to the transition point is 25.0, as shown in Fig. 5(b). This means when the transition happens, the strength of the drag momentum is at least one order larger than the strength of the thrust momentum since the propeller effect is very weak at low rotation speed. Under such a condition, the drag momentum is dominant to the total momentum (or called net momentum). It is very similar to that of a towed sphere without propeller, particularly for the linearly growth of wave amplitude versus Fr.

For the second case in Fig. 5(d), the J_{nd} value corresponding to the transition point is 2.0. At first, the drag momentum is bigger but not dominant and the total momentum is remarkably weakened by the thrust momentum, which suppresses the growth of the wave amplitude. Then when the J_{nd} value grows up to 10, indicating that the drag momentum becomes dominant, the wave amplitude clearly starts to increase.

For the third case shown in Fig. 5(f), the J_{nd} value associated with Fr_{c} is 0.4 and even the maximum J_{nd} is only 4.0, which means the drag momentum is never dominant in the total momentum. This is the reason why the wave amplitude has no explicit increase.

Thus, for the wake-generated IWs after the transition, we think the J_{nd} value ranging from 1 to 10 should be a region of zero-momentum wake. In this region, the momentum difference generated by the bluff body and the propeller is too small to produce effective large-scale structure and thus no large amplitude IWs can be excited.

2.3 Wave Patterns

The wave patterns in the horizontal plane are the most essential issue of IWs concerned in the previous studies. The electrical signals of conductivity probes can be converted to the fluctuations of density using the relations calibrated before the experiments. The wave patterns at a depth (z) of 25 cm are shown in Figs. 6 and 7. The gray-scale contour maps are obtained by utilizing the interpolation with the first set of probes. The horizontal axis is the width of tank, and it ranges

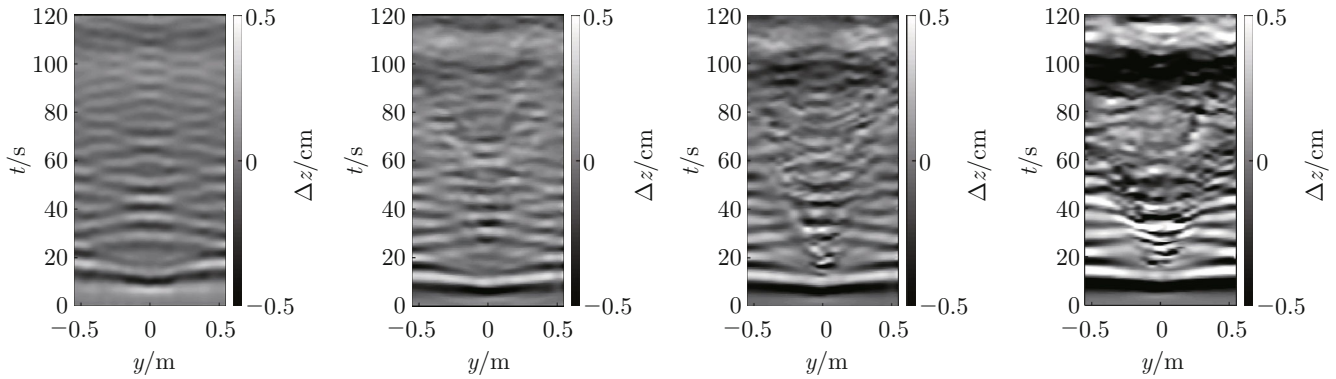

(a) $J_{\mathrm{T}}=0\ \mathrm{m^4/s^2}$, $Fr=1$ (b) $J_{\mathrm{T}}=1.9\times10^{-5}\ \mathrm{m^4/s^2}$, $Fr=1$, $J_{\mathrm{nd}}=2.25$ (c) $J_{\mathrm{T}}=1.7\times10^{-4}\ \mathrm{m^4/s^2}$, $Fr=1$, $J_{\mathrm{nd}}=0.25$ (d) $J_{\mathrm{T}}=1.1\times10^{-3}\ \mathrm{m^4/s^2}$, $Fr=1$, $J_{\mathrm{nd}}=0.06$

Fig. 6 The wave patterns in the horizontal plane before the transition

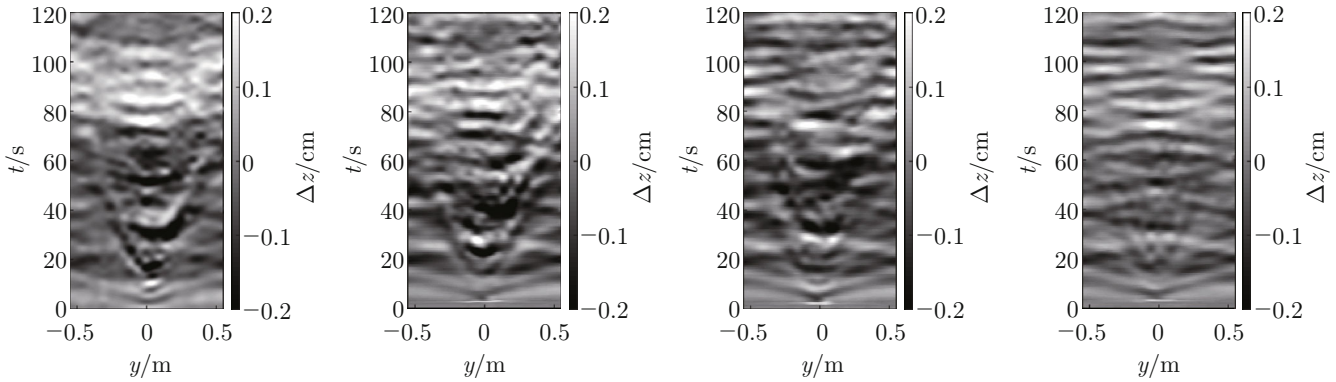

(a) $J_{\mathrm{T}}=0\ \mathrm{m^4/s^2}$, $Fr=6$ (b) $J_{\mathrm{T}}=1.9\times10^{-5}\ \mathrm{m^4/s^2}$, $Fr=6$, $J_{\mathrm{nd}}=81$ (c) $J_{\mathrm{T}}=1.7\times10^{-4}\ \mathrm{m^4/s^2}$, $Fr=6$, $J_{\mathrm{nd}}=9$ (d) $J_{\mathrm{T}}=1.1\times10^{-3}\ \mathrm{m^4/s^2}$, $Fr=6$, $J_{\mathrm{nd}}=2.25$

Fig. 7 The wave patterns in the horizontal plane after the transition

from −0.55 to 0.55 m. The vertical axis represents the time (t) with a period of 120 s, where $t = 0$ is the beginning of wave fluctuation. The gray-scale range (Δz) is fixed at ±0.5 cm for Fig. 6, and ±0.2 cm for Fig. 7.

Figure 6 shows the wave patterns before the transition for Fr at 1. One can clearly find that the propeller performs wake effect on the IWs. In Fig. 6(a), the slender model is purely towed without the propeller effect, i.e., J_{T} is zero, and the IW generated by the pure body effect is a symmetric V-shaped wave with a large opening angle. For the other three cases in Figs. 6(b)—6(d), a narrower V-shaped wave pattern can be observed in each sub-figure, and it is a signature of the wake-generated IWs[2,8]. According to the previous studies, the wake generated by the moving model is very weak at such a low speed and cannot form any significant wave signatures. Therefore, the narrower inner V-shaped patterns in Figs. 6(b)—6(d) must be excited by the wake from the propeller. They should not be formed if the model is purely towed.

The propeller also affects the body effect simultaneously. Despite the inner V-shaped patterns, the contrast of wider V-shaped patterns generated by the pure body effect becomes more obvious with the increase of J_{T} in the contour maps of Figs. 6(b)—6(d). This means the overall waves have larger peaks and smaller valleys with the increase of J_{T}, and the IW peak-peak amplitude increases with the increase of J_{T} for the same Fr. The reason is that the rotating propeller acts as a volume source attached to the body and enhances the body effect on the body-generated IWs. Higher rotation speed of the propeller means larger body effect and leads to higher wave amplitude.

Figures 7(a)—7(d) show the wave patterns after the transition for Fr at 6, where the outer and inner V-shaped patterns appear simultaneously under different J_{T}. The outer V-shaped patterns which are the signatures of the pure body effect waves share the same bright and dark contrasts in each sub-figure, indicating that the body effect keeps nearly unchanged after the transition. Meanwhile, the inner V-shaped patterns show clear discrepancies in the contrasts. It is noted that the most obvious contrast does not appear in Fig. 7(d) under the largest J_{T} but in Fig. 7(b) under the largest J_{nd}, unlike the situation for the cases before the transition.

This is the result of the balancing and cancelling dynamics between J_{D} and J_{T}. As discussed in Subsection 2.2, the net value of the total momentum is determined by the difference between J_{D} and J_{T}. Higher J_{nd} means stronger total momentum, leading to larger peak and valley of the IWs.

Moreover, the problem of the propeller action in the IW generation can be very interesting. If any proper spectrum analysis can be developed to decompose the wave patterns, the more useful information can be revealed to advance the understanding of the dynamics. Unfortunately, such a method is still absent and it may be the key to the further research.

3 Conclusion

In this paper, the characteristics of IWs generated by the towed model with rotating propeller in a strongly stratified fluid are investigated experimentally. A model with an aspect ratio of 8 is towed at the speed ranging from 10 to 120 cm/s, while its propeller works behind. The characteristics of the IWs are analyzed and discussed on the basis of conductivity signal histories recorded by the arrays of probes.

The results of the along-track speeds of the IWs are obtained from cross correlation analysis, and the characteristics of the IW transition are investigated. Two types of the wave exciting sources are distinguished: the body effect and the wake effect. The transition occurs for Fr_{c} at 3.3, 3.0 and 2.7 corresponding to J_{T} at 1.9×10^{-5}, 1.7×10^{-4} and 1.1×10^{-3} m^4/s^2 respectively, indicating that the growing strength of the propeller wake advances the transition from the body-generated IWs to the wake-generated IWs.

Before the transition, the propeller performs the body and wake effects simultaneously. The body effect enlarges the wave amplitude and raises the contrast of the wave pattern contour maps. It also amplifies the wave amplitude and acts as a coefficient in the relation of A_{m}/D versus Fr. The wake effect excites the narrower inner V-shaped patterns in the wave patterns that should not be formed if the model is purely towed at very low speed.

After the transition, the IW characteristics are also changed a lot by the propeller. In three cases with different J_{T} values, the variations of their maximum peak-peak wave amplitudes are different from each other. The first case shows a linear growth in wave amplitude with J_{nd} exceeding 10, like the situation of a towed model. The wave amplitude in the second case does not rise at first but begins to grow nearly for J_{nd} at 10. In the third case, it continues to decrease after the transition and does not have an obvious increase. The difference results from the balancing and cancelling interaction between J_{D} and J_{T} provided by the model body and the propeller action, respectively. Influence of such a dynamic also appears in the wave patterns that the highest contrast does not appear under the largest J_{T} but under the largest J_{nd}. We think the J_{nd} value ranging from 1 to 10 is a region of zero-momentum wake, where the total (net) momentum is too small to excite large amplitude IWs.

The experimental results preliminarily show that the IWs generated under the propeller effect have great difference with those excited by the towed model. However, due to the limitation of the experimental

conditions and techniques, it is hard to evaluate the propeller effect quantitatively. With the improvement of experimental methods and facilities, further research will focus on the transportation mechanism of IWs and contribute to the theoretical model of propeller effect, advancing the wake detection technology of underwater vehicles.

References

[1] KELLER J B, MUNK W H. Internal wave wakes of a body moving in a stratified fluid [J]. *Physics of Fluids*, 1970, **13**(6): 1425-1431.

[2] ROBEY H F. The generation of internal waves by a towed sphere and its wake in a thermocline [J]. *Physics of Fluids*, 1997, **9**(11): 3353-3367.

[3] HOPFINGER E J, FLOR J B, CHOMAZ J M, et al. Internal waves generated by a moving sphere and its wake in a stratified fluid [J]. *Experiments in Fluids*, 1991, **11**(4): 255-261.

[4] BONNETON P, CHOMAZ J M, HOPFINGER E J. Internal waves produced by the turbulent wake of a sphere moving horizontally in a stratified fluid [J]. *Journal of Fluid Mechanics*, 1993, **254**: 23-40.

[5] LIN Q, BOYER D L, FERNANDO H J S. Internal waves generated by the turbulent wake of a sphere [J]. *Experiments in Fluids*, 1993, **15**(2): 147-154.

[6] CHOMAZ J M, BONNETON P, HOPFINGER E J. The structure of the near wake of a sphere moving horizontally in a stratified fluid [J]. *Journal of Fluid Mechanics*, 1993, **254**: 1-21.

[7] DUPONT P, VOISIN B. Internal waves generated by a translating and oscillating sphere [J]. *Dynamics of Atmospheres and Oceans*, 1996, **23**: 289-298.

[8] WANG H, CHEN K, YOU Y. An investigation on internal waves generated by towed models under a strong halocline [J]. *Physics of Fluids*, 2017, **29**(6): 065104.

[9] SCHOOLEY A H, STEWART R W. Experiments with a self-propelled body submerged in a fluid with a vertical density gradient [J]. *Journal of Fluid Mechanics*, 1963, **15**: 83-96.

[10] GILREATH H E, BRANDT A. Experiments on the generation of internal waves in a stratified fluid [J]. *AIAA Journal*, 1985, **23**(5): 693-700.

[11] VOROPAYEV S I, MCEACHERN G B, FERNANDO H J S, et al. Large vortex structures behind a maneuvering body in stratified fluids [J]. *Physics of Fluids*, 1999, **11**(6): 1682-1684.

[12] MEUNIER P, SPEDDING G R. Stratified propelled wakes [J]. *Journal of Fluid Mechanics*, 2006, **552**: 229-256.

[13] BRUCKER K A, SARKAR S. A comparative study of self-propelled and towed wakes in a stratified fluid [J]. *Journal of Fluid Mechanics*, 2010, **652**: 373-404.

[14] WANG H W, CHEN K, YOU Y X, et al. Experiments on internal waves generated by a self-propelled model in a stratified fluid [C]//*Proceedings of the 27th International Ocean and Polar Engineering Conference*. San Francisco, USA: International Society of Offshore and Polar Engineers, 2017: 817-822.

[15] VOROPAYEV S I, MCEACHERN G B, FERNANDO H J S, et al. Large vortex structures behind a maneuvering body in stratified fluids [J]. *Physics of Fluids*, 1999, **11**(6): 1682-1684.

[16] VOROPAYEV S I, SMIRNOV S A. Vortex streets generated by a moving momentum source in a stratified fluid [J]. *Physics of Fluids*, 2003, **15**(3): 618-624.

[17] VOROPAYEV S I, FERNANDO H J S, SMIRNOV S A, et al. On surface signatures generated by submerged momentum sources [J]. *Physics of Fluids*, 2007, **19**(7): 076603.

[18] CHEN K, YOU Y, NOBLESSE F. Experimental study of quasi-2D dipolar vortex streets generated by a moving momentum source in a stratified fluid [J]. *Physics of Fluids*, 2016, **28**(7): 075105.